Int. J. Electrochem. Sci., 10 **(2015)** 6213 - 6226

International Journal of
ELECTROCHEMICAL
SCIENCE
www.electrochemsci.org

Reduced Graphene Oxide Sheets with Added Pt-Pd Alloy Nanoparticles as a Good Electro-catalyst for Ethanol Oxidation

Mohammad Faruk Hossain[*] *and Jae Yeong Park*

Micro/Nano Devices & Packaging Lab., Department of Electronic Engineering, Kwangwoon University, 447-1, Wolgye-Dong, Nowon Gu, Seoul, 139-701, Korea
[*]E-mail: jaepark@kw.ac.kr

Received: 19 February 2015 / *Accepted:* 21 May 2015 / *Published:* 24 June 2015

This work investigates the use of platinum and palladium alloy nanoparticles (PtPdNPs) embedded on highly hybridized reduced graphene oxide sheets (RGOs) as an excellent anode catalyst for ethanol oxidation. Cyclic voltammetery and the amperometric method were applied to evaluate the catalytic performance of the modified electrodes in terms of the electrocatalytic oxidation of ethanol. RGOs/PtPdNPs catalysts exhibited much higher catalytic activity and current density than monometallic nanoparticle catalysts in an alkaline solution. The current density of RGOs/PtPdNPs catalyst was measured of 120.2 mA/cm^2, moreover, the onset potential of this electrode was of -0.671 mV with a forward and backward current ratio of 1.7. These results reveal that the catalyst electrode has good electrocatalytic activity and a moderate tolerance in opposition to the poisoning by intermediates formed during the ethanol electroxidation.

Keywords: Reduced graphene oxide sheets (RGOs), PtPd nanoparticles, Electrochemical, Ethanol electro-oxidation.

1. INTRODUCTION

Over the last decade, fuel cells have attracted extensive attention as a substitute energy sources due to the decreasing desire to rely on petrifaction fuels and the increase in environmental contamination. Several types of fuel cells are available for energy sources, and among them, direct alcohol fuel cells (DAFCs) are considered to be a sustainable energy source for applications in bearable electronic instruments and transportation [1-2]. Recently, direct ethanol fuel cells (DEFCs) have drawn much observation since ethanol is enormous, non-toxic and cheap. Besides, the energy density of ethanol is higher than that of methanol. However, the fruitful commercialization of DEFCs depends on the stability and performance of the electrocatalyst.

Thus, in order to enhance the activity of the cells, it is important to develop a novel anodic catalyst for ethanol oxidation. Platinum is one of the most commonly used catalysts in DEFCs, but it is too expensive. Therefore, Pt–Pd nanoparticle catalysts have been mainly used in such devices for several reasons. First, the properties of Pt are very identical to those of Pd concerning of having a uniform face centred cubic (fcc) crystal structure and an atomic size with a distinction of only 3%, and Pd has ability to make alloy with Pt in terms of any atomic ratio [3]. Second, since Pd is more plenty (approximately over 50 times) on the Earth and is inexpensive than Pt, a Palladium based catalyst is thought to be a suitable alloy element for Pt in DEFCs [4-5]. Third, a bimetallic Pt–Pd system with an appropriate atomic ratio can exhibit a higher obstruction against CO poisoning for the oxidation of a few organic molecules, such as formic acid [6]. In addition, trimetallic or bimetallic materials, which synergistically improved the performance, have been used in electronic, electrocatalytic, and magnetic applications [7].

To improve the catalytic performance of the electrocatalysts, a proper base structure is required that can contribute an efficient dispersion of the catalyst particles. So, reduced graphene oxide (RGO), a flat graphite monolayer packed into a two-dimensional honeycomb lattice, is a good choice for such purposes. RGO has a good caliber to stimulate rapid electron transfer for a broad area of electroactive molecules when it is acted as an electrode substrate [8]. Metal nanoparticles on RGO can conduct to a nanocomposite with a wider specific surface area and acted good electron conduction path way that can enhance the electrocatalytic reactions.

However, RGO are still remained some faults, such as a large amount of residual oxygen groups [9], and a highly decomposed and disordered structures are far from pristine graphene. Anyway, the availability of oxygen bearing groups on its plane or at the edges is sometimes beneficial because it can notably influence the interfacial action between the electrolyte and the graphene modified electrode. Regarding the reduced graphene oxide structure, the oxygen-bearing groups, such as hydroxyl groups and epoxy at the basal plane, whereas carbonyl group at the edges, can act as anchoring sites to attach other materials, such as polymers, metal oxides, nanoparticles [10-12].

Moreover, oxygen-bearing groups in RGO may distribute as reactive sites that can enhance the oxygen groups at the electrode interface, which can then accelerate the oxygen reduction reaction (ORR) [13]. On the contrary, the availability of more surface oxygen containing groups affects the conductivity of the RGO sheets [14]. For example, the inclusion of heteroatom-like oxygen can decrease the electron or the hole movability and can increase the resistivity. Concerning this limitation, it is important to control the density of oxygen-bearing groups in RGO sheets in order to achieve maximum performance. As a result, many efforts have been exerted toward developing RGO fabrication techniques through a variety of chemical, thermal, and electrochemical process [15-17].

In this work, RGO suspension is cast on a substrate electrode and is dried at ambient temperature. RGO-modified electrode is then thermally treated, and a bimetallic PtPdNPs is deposited on the prepared electrode to enhance its electrocatalytic performance for ethanol oxidation in alkaline solution. The as-prepared anode catalyst is evaluated by measuring its catalytic performance as well as its carbonaceous intermediate tolerance during the ethanol electro-oxidation reaction.

2. EXPERIMENTAL

2.1 Chemicals and instruments

Hexachloroplatinic acid (H_2PtCl_6), Palladium (II) chloride ($PdCl_2$), and graphite powder (particle size of 44 μm) were bought from Sigma-Aldrich Co. (South Korea). Chemicals used in the experiment were an analytical grade, and the electrochemical behaviors (cyclic voltammetry and chronoamperometry) for the developed electrodes were conducted in a three electrodes system by using an electrochemical analyzer (CH Instruments Inc., Model 600D). An Hg/HgO with 1 M of NaOH and a flat Pt bar were utilized as a reference electrode and counter electrode, respectively. All potentials reported in cyclic voltammetry (CV) are relative to the Hg/HgO reference electrode, and current densities in CV and chronoamperometry are presented per geometric area.

Fabricated electrodes, RGO and Graphite oxide were physically characterized via FESEM with EDX (Hitachi S-4300), Fourier transform infrared spectroscopy (FTIR; NICOLET560, Nicolet), and high-resolution X-ray photoelectron spectroscopy (XPS; ULVAC-PHI PHI-5000).

To provide the morphological analysis of the surface using FESEM, samples with a size of 4 mm x 5 mm were fixed with conductive carbon tape on an aluminum stub, and a 15 kV accelerating voltage was applied, and the surfaces of the modified electrodes were observed and photographed. Then, similarly prepared samples were subjected to EDX with a beam voltage of 20 kV and an acquisition time 300 s to perform the elemental analysis.

Samples under FTIR analysis were performed on a SPECTRUM 100 Fourier transform infrared spectrophotometer at a resolution of 4 cm^{-1} with an accumulation of hundred scans for each spectrum and the infrared spectra were noted in absorbance units in the 4000–400 cm–1 range. The FTIR spectra were analyzed in potassium bromide pellets containing 1% fine powder samples. Al Kα radiation (1486.7 eV) with pass energy of 23.4.0 eV and a power of 23.4 W used in XPS were conducted to characterize graphite oxide (GO) and reduced graphene oxide sheets (RGOs).

2.2 Preparation of GO and RGO platelets

GO was synthesized according to modified Hummers method [18-19]. GO platelets were obtained after drying the precipitation, and then 50 mg of GO were dispersed into 30 mL of ethylene glycol, pursued with sonicator for 2 hours (h). Then, 40 mL of ultrapure water were dropped to the solution and continued stirring for 1 h. After that, 270 mg of $NaBH_4$ were gradually mixed, and then the mixture of the solution was heated at 110 °C for 2 h. Then, the solution mixture was filtered, washed several times with ultrapure water and finally, filtered material was heated up overnight in an oven at 95 °C under vacuum.

2.3 Fabrication of RGO sheets-modified electrodes

To fabricate the nano-formed electrodes, a titanium layer of 70 nm was sputtered on top of a Si/SiO_2 substrate. A gold layer of 200 nm was sputtered on thin titanium layer. Gold thin layer was

conducted as a seed layer for the developed hybrid electrode catalyst. The electrodes in size (5 mm X 4 mm) were made by photolithographic technique. 20 mg of RGO platelets were dispersed in 20 mL of dimethylformamide and ultrapure water (1:1) solution. Then, the mixture was sonicated at 200 W for 3 h. Finally, 15 µL of the sonicated RGO suspension were dropped on the surface of Au thin layer and kept under ambient conditions. After drying, Au thin electrode decorated with the RGO was cleaned with phosphate buffered saline solution and ultrapure water, and were subsequently dried with N_2 gas. The RGO modified electrode was then kept in a vacuum oven at 155 °C to recover the defect sites of the RGO sheets and to enhance the adhesion between the RGOs and Au.

2.4 Fabrication of RGOs/PtPdNPs - modified Au thin film electrode

An Hg/HgO as a reference electrode, a platinum sheet as a counter electrode, and the modified thin film Au electrode as the working electrode were used for a traditional three electrodes system. PdPtNPs were deposited on the surface of the treated RGOs via electrodeposition at a constant potential of -0.2 V in a Pt and Pd precursors solution that contain 2.5 mM of $PdCl_2$, H_2PtCl_6 (1:1), and 0.1 M KCl for 60 s, 90 s and 120 s at 55 mC charge conditions. Afterward, the electrodes were cleaned with ultrapure water and dried with nitrogen gas. Monometallic nanoparticles were also formed on the RGOs-modified electrodes under the same conditions. Fig. 1 shows the rectangular design of electrode (A) and the schematic diagrams of the fabrication procedures for RGOs/PtPdNPs-modified hybrid electrodes (B). It is worth-nothing that we experimented only with the nanoparticles modified hybrid electrodes that had undergone 90 s of deposition time because the electrodes with 60 s depositions exhibited less catalytic activity. On the other hand, 120 s nanoparticle depositions produced clusters on the surface of the electrodes.

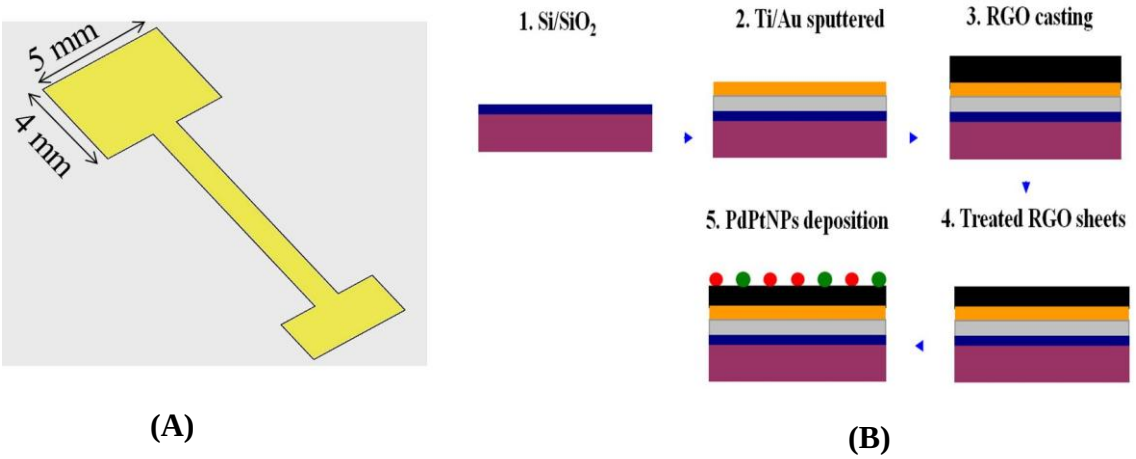

Figure 1. (A) Rectangular design of thin film electrode and (B) Schematic drawing of the fuel cell anode electrode catalysts.

3. RESULTS AND DISCUSSION

3.1 Physical properties of GO and RGO sheets

The surface morphology of the developed reduced graphene oxide sheets (RGOs) and the nanoparticles decorated RGOs-modified electrodes are shown in Fig. 2. The FESEM image of RGOs formed after three hours of ultrasonication and drying at room temperature is clearly visible in Fig. 2A. Few layers of RGO sheets were dropped-cast on the Au thin layer, and a typical wrinkle of RGO sheets formed during the chemical reduction has been seen.

Fig. 2B shows the FESEM image of the RGO sheets formed via heat treatment. A typically large number of small wrinkles on the RGO sheets can be seen to have formed after heat treatment. These curls indicate that the imperfection and the remaining oxygen functional groups in RGO sheets have been largely removed during heat treatment [20]. The geometric crumpling not only decreases the surface energy but also influences a good film-forming ability as a result of nano-scale sheet interlocking [21]. When RGOs were further modified with the nanoparticles, the nanoparticles cover all of RGOs, and these make rougher, with more electro active sites and larger active surface area.

Fig. 2C shows the FESEM image of RGOs with PtNPs deposited for 90 s. In this figure, the particles distribution of PtNPs on RGOs-modified electrodes can be seen to be irregular. Some Pt nanoparticles have agglomerated (over plated) and some are generated on the electrode surface. These observations indicate that as time passes, reduced Pt seeds are plated on the generated nucleus until repulsion occurs, and after repulsion, a new nucleus may be generated on the electrode surface. Since Pt is a noble metal, reduced Pt seeds are plated directly on the generated nucleus rather than forming a new nucleus.

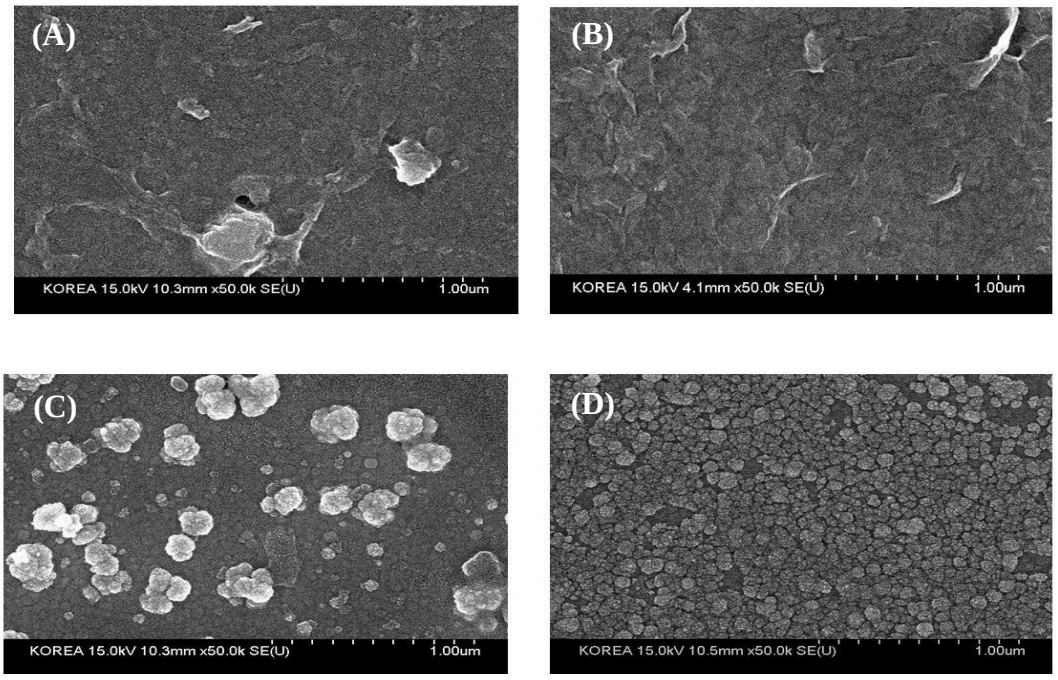

Figure 2. FESEM images of (A) RGO sheets, (B) RGO sheets after heat treatment, (C) RGOs/PtNPs, and (D) RGOs/PdNPs.

The particles size of PtPdNPs is smaller than that of Pd nanoparticles (Fig. 2D and 3A). A decrease in the particle size of the PtPdNPs may form a PtPd alloy on the RGOs [22] which indicates that Pt and Pd were simultaneously plated out onto the electrode surface. Fig. 3A also shows a uniform distribution of the PtPdNPs on RGOs, which contributes a good platform for electrochemical applications [23].

The compositions of RGOs/PtPdNPs-modified electrode were conducted via EDX, as shown in Fig. 3B. The elemental peaks for Pt, Pd, C, and O were found in the RGO/PtPdNPs. The percentage of loading C, O, PtNPs, and PdNPs in RGOs/PtPdNPs were 65.34%, 15.09%, 11.87%, and 7.7%, respectively. These results indicate that a higher percentage of PtNPs than PdNPs was co-deposited as a result of the electrostatic interaction of the negatively charged RGOs. The likely reason for this phenomenon is that the negatively charged $PtCl6^{2-}$ ions easily formed in the concentrated chloride media, but the positively charged Pd^{2+} ions were not easily formed. These ions would then be formed the PtPd nanoparticles [24]. Nevertheless, this ensures that the PtPdNPs successfully formed under the indicated environments, and that both particles donate towards the creation of the modified electrode for ethanol oxidation.

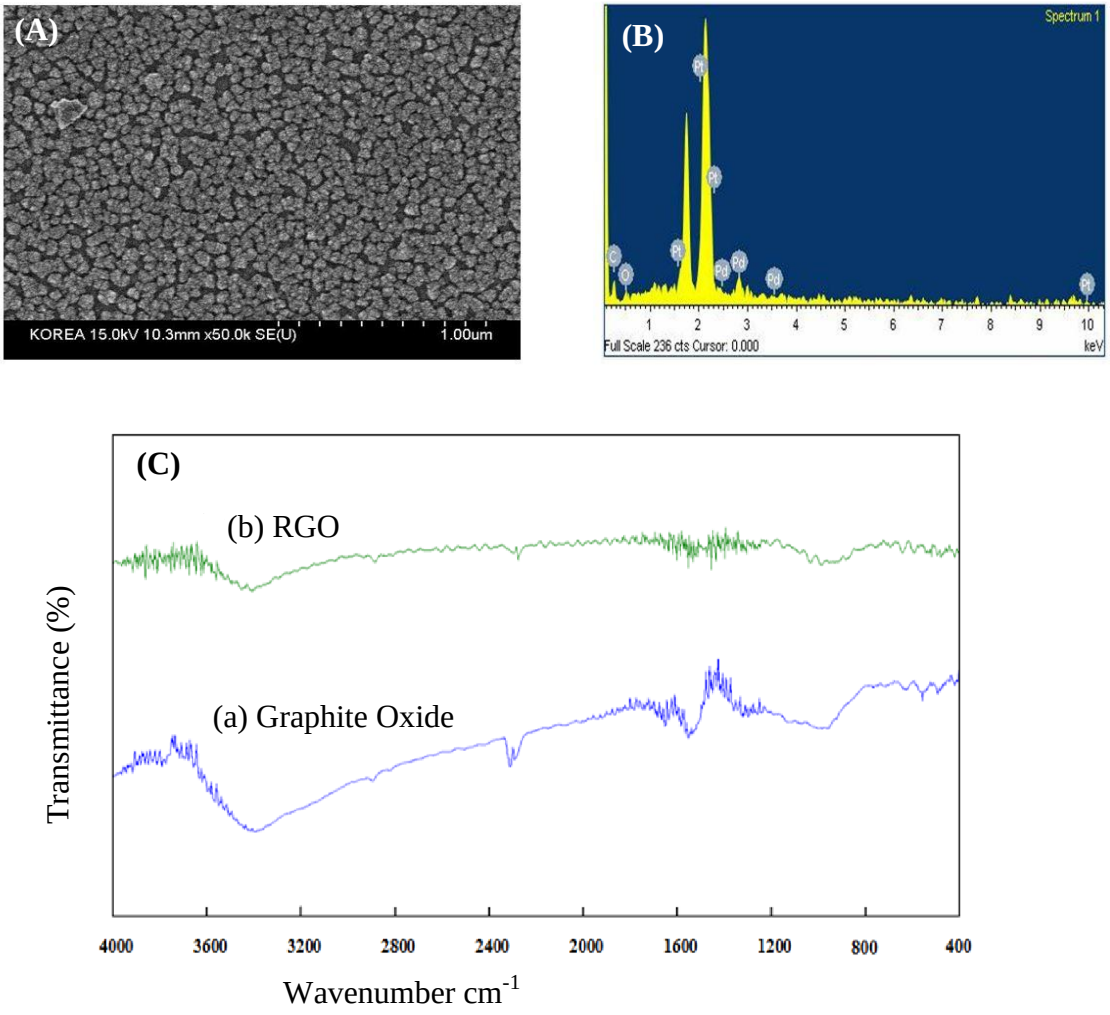

Figure 3. (A) FESEM images of RGOs/PtPdNPs, (B) respective EDX spectrum of RGOs/PtPdNPs, and (C) FTIR spectra of (a) GO, and (b) RGO platelets.

The FTIR analysis is conducted to acquire the infrared absorption spectrum of the solid. RGO and GO powder were used to characterize infrared absorption via FTIR analysis. The spectra express the availability of different types of bonds in RGO and GO.

The FTIR spectra of RGO and GO platelet powder are shown in Fig. 3C. The major peaks for GO created at 1080.6 cm^{-1}, 1382.2 cm^{-1}, 1629.5 cm^{-1}, 1709.4 cm^{-1}, and 3410.0 cm^{-1}. The peak arises at 3410.0 cm^{-1} due to -OH stretching vibration, whereas the peak observes at 1709.4 cm^{-1} resulting from the C=O stretching vibration. The peak at 1629.5 cm^{-1} is imposed on the O–H bending vibration of the sunk water molecules and to the performances from the vibration of aromatic C=C. Another two peaks at 1382.2 cm^{-1} and 1080.6 cm^{-1} generates from the deformation vibration of -OH and the C-O stretching vibration of the alkoxy groups as shown in Fig 3C (a) [25-26].

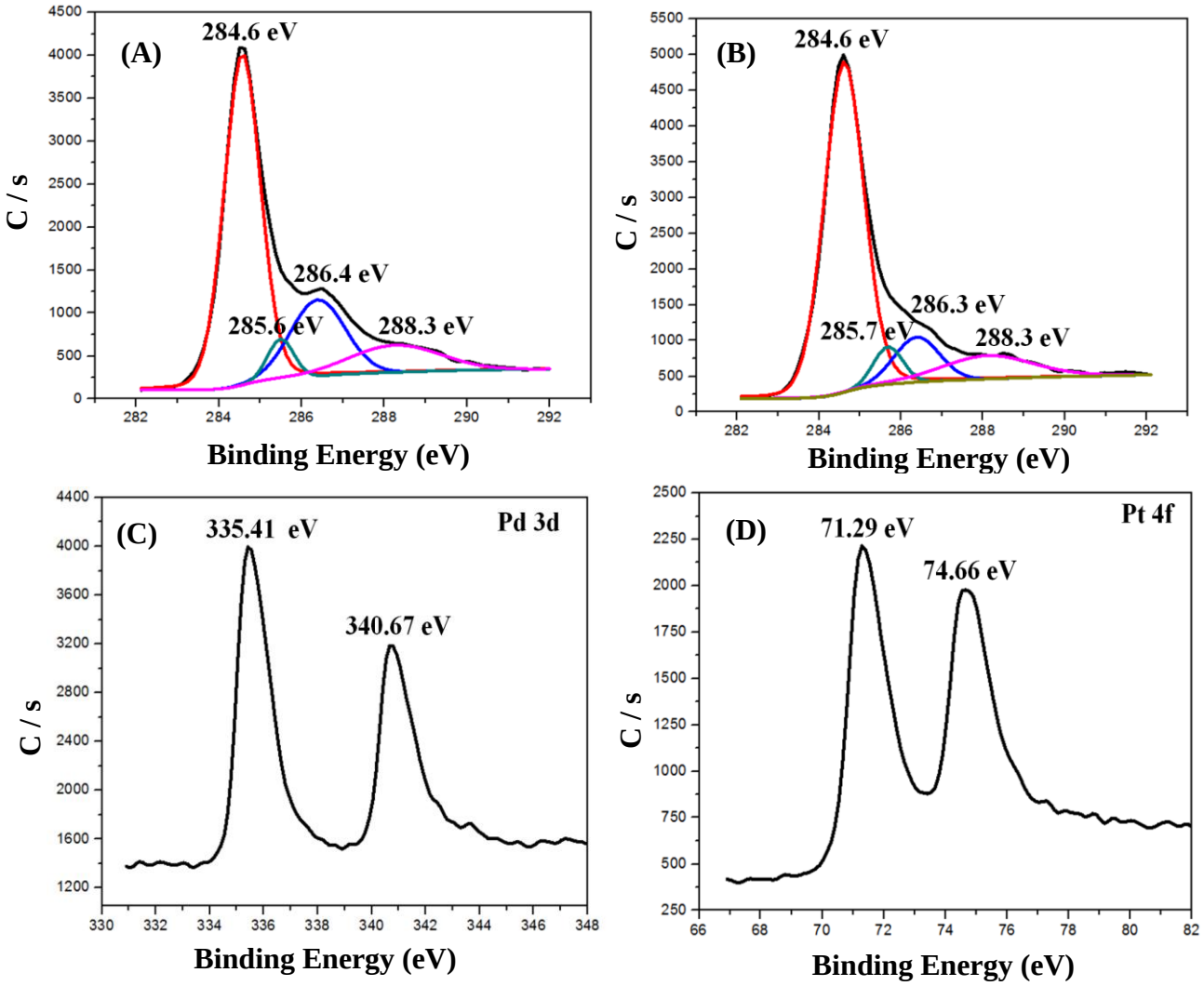

Figure 4. XPS spectrum of (A) RGO platelets, (B) RGO sheets on Au electrode after heat treatments, (C) XPS spectra of Pd nanoparticles into RGOs/PtPdNPs, and (D) XPS spectra of Pt nanoparticles into RGOs/PtPdNPs.

The main peaks for RGO generated at 1419.9 cm^{-1}, 1577.7 cm^{-1}, 1624.2 cm^{-1}, 1718.5cm^{-1}, and 3421.7 cm^{-1}. The peaks observes at 3421.7 cm^{-1} and 1718.5 cm^{-1} due to the consequence of the -OH

stretching vibration and the C=O stretching vibration, respectively as shown in Fig. 3C (b). The peak displays at 1624.2 cm^{-1} resulting the O–H bending vibration of the sunk water molecules and in the consequence from the vibration of the aromatic C=C. The deformation vibration of –OH creates at 1419.9 cm^{-1}, and RGO is assigned to the C = C skeletal vibration of graphene sheets at 1577.7 cm^{-} [27-28], which ensures the successful reduction of GO.

The C1s XPS spectra of RGO platelets and RGOs are exhibited in Fig. 4A and 4B, respectively, which are clearly visible a considerable degree of oxidation with respect to the carbon atoms in several functional groups.

The non-oxygenated C ring (284.6 eV) that involves a C=C bond produces sp^2 hybridization, the C in the C–O bonds (286.2 eV) that involves epoxy groups and hydroxyl. On the contrary, the C in C=O bonds (288.2 eV) that comprises the carbonyl groups [29-30]. Another peak (285.6 eV) is sp^3 hybridized and involves a C-C bond [15]. Fig. 4A and 4B indicate that the peaks of the oxygen functional groups have decreased and the non-oxygen functional group peaks have increased for the RGO sheets on an Au substrate. RGOs were greatly improved by further modification through heat treatment, and the results can be seen in the FESEM image in Fig. 2B.

XPS was also conducted to observe the composition of the PtPd bimetallic alloy on the RGOs-modified electrode. The Pd 3d and Pt 4f spectra of the sample are shown in Figs. 4C and 4D, respectively. Pd 3d has two peaks for 3d5/2 and 3d3/2 with binding energies at 335.41 eV and 340.67 eV, respectively, as shown in Fig. 4C. Pt 4f also has two peaks for 4f7/2 and 4f5/2 at 71.29 eV and 74.66 eV, respectively, as seen in Fig. 4D. The results are consistent with those from previous reports [22, 24], and this further confirms that the PtPd bimetallic alloy nanoparticles have been effectively co-deposited under the given environments onto RGOs-modified electrode.

3.2 Electrochemical characterization

The electrocatalytic activities for ethanol oxidation by the Au/PtPdNPs, RGOs/PtPdNPs, RGOs/PtNPs and RGOs/PdNPs catalysts were evaluated by using cyclic voltammogram (CV) in 0.5 M NaOH + 2 M ethanol using a scanning rate of 50 mV/s, as shown in Fig. 5A. The developed catalysts demonstrate well-parted anodic peaks in the forward and backward sweeps due to ethanol oxidation. The forward oxidation anodic peak (f) is generally accepted to be assigned to the oxidation of again chemisorbed species proceeding from ethanol adsorption, and the backward oxidation peak (b) is basically related to the removal of carbonaceous species that are not fully oxidized in the anodic scan, but are rather resulted from newly chemisorbed species [31].

The CV curves of PtPd alloy nanoparticles on RGOs modified electrode and plain thin gold electrode displays in 0.5 M NaOH solution at a scan rate of 50 mV/s as in Fig 5B. Based on a previous report [32], the mechanism for ethanol oxidation on the nanoparticles catalysts can be demonstrated through the following Equations:

$$CH_3CH_2OH \leftrightarrow (CH_3CH_2OH)_{ads} \quad [1]$$

$$(CH_3CH_2OH)_{ads} + 3OH^- \rightarrow (CH_3CO)_{ads} + 3H_2O + 3e^- \quad [2]$$

$$OH^- \leftrightarrow OH_{ads} + e^- \quad [3]$$

$$(CH_3CO)_{ads} + OH_{ads} \rightarrow CH_3COOH \quad [4]$$

$$CH_3COOH + OH^- \rightarrow CH_3COO^- + H_2O \quad [5]$$

Thus, more generated OH^- can produce a plenty of OH_{ads}, which can remarkably stimulate Equations (2–4). As a result, the process for the ethanol oxidation reaction (EOR) was effectively formed, leading to a raised peak current for EOR. The current density of PtPdNPs decorated RGOs modified catalysts is higher than that of PtNPs decorated RGOs and PdNPs decorated RGOs modified catalysts due to the synergistic effect of the two elements as shown in Fig. 5A. This consequence is obviously due to the alteration in the geometrical structure (e.g., a reducing distance in the Pt–Pt bond) or an electronic effect (e.g., an enhancement of Pt d-electron vacancies), in this case one element changes the electronic properties and other one generates a more active catalytic surface [18]. The maximum current densities are 120.2 mA/cm^2 at 0.13 V, 97.37 mA/cm^2 at 0.12 V, 53.02 mA/cm^2 at 0.028 V, and 11.44 mA/cm^2 at -0.16 V. for RGOs/PtPdNPs, Au/PtPdNPs, RGOs/PdNPs and RGOs/PtNPs, respectively, which reflects the size and distribution of the NPs.

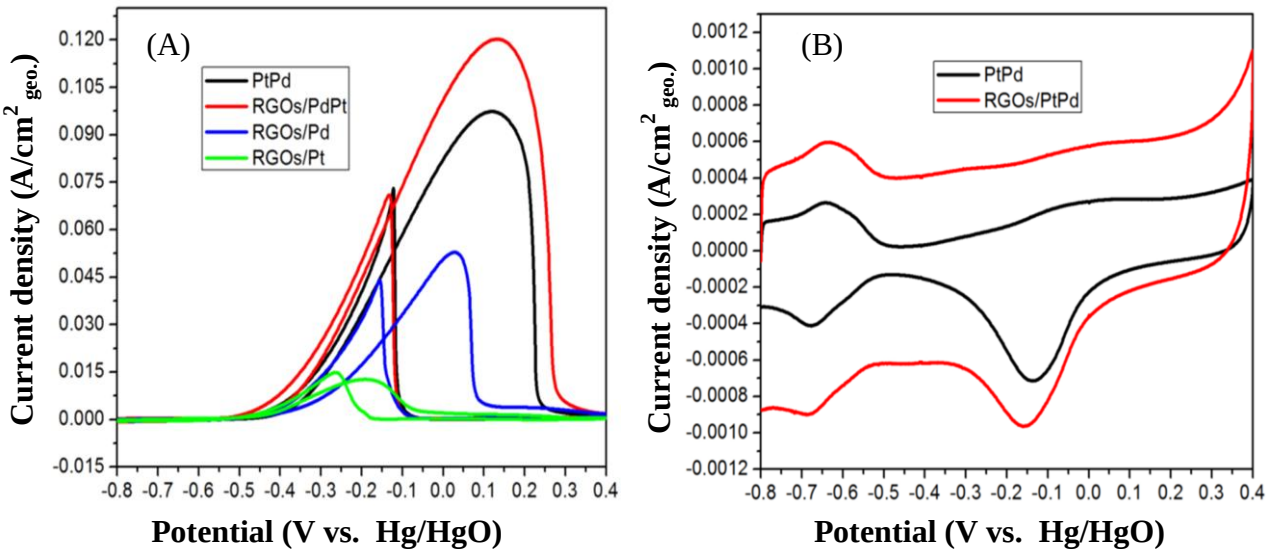

Figre 5. Cyclic voltammetry (CV) of the developed catalysts on RGOs-modified and bare plain electrodes in 0.5 M NaOH + 2 M ethanol solution (A), CV curves of PtPd alloy nanoparticles on RGOs modified electrode and bare plain electrode in 0.5 M NaOH solution (B).

The activity of catalyst is evaluated by using onset potential, which is one of the key parameters. The activity of the RGOs/PtPdNPs catalyst was exhibited to be around -0.671 mV (vs. Hg/HgO), which is considerably smaller than those of the other two mono-metallic catalysts. The results reveal that a large amount of hydroxide was adsorbed by the effective surface area of the RGOs/PtPdNPs catalyst during CV scanning, which is in good agreement with Equations (2-4). As a result, RGOs/PtPdNPs catalyst significantly improved the EOR in the respective solution. To

understand the action of RGO in the catalytic reaction, a cyclic voltammogram for the PtPdNPs-modified electrode was captured in 0.5 M NaOH + 2 M ethanol solution, which is clearly shown in Fig. 5A. The maximum current density of RGOs/PtPdNPs (120.2 mA/cm^2) is seen to be higher than that of Au/PtPdNPs (97.37 mA/cm^2). The onset potential of Au/RGOs/PtPdNPs catalyst was originated at around -0.671 V (vs. Hg/HgO) whereas Au/PtPdNPs catalyst showed -0.63 V (vs. Hg/HgO). These results indicate that some defect sites are likely to still remain after the RGO sheets were treated. These defect sites would adsorb the OH molecules formed by water dissociation during CV scanning. As a result, RGOs may significantly enhance the ethanol oxidation with the help of PtPd alloy nanoparticles, which is ascribed to the excellent charge transfer phenomena of RGO sheets [24, 2].

The ratio of the forward peak current density to the backward reverse peak current density (f/b) was used to determine the poisoning tolerance due to the intermediate species. The f/b ratio of RGOs/PtPdNPs samples is 1.7, which is higher than that of individual monometallic catalyst and the bare electrode with PtPdNPs. This ratio shows that RGOs/PtPdNPs samples have good tolerance against intermediate poisons. Fig. 5B shows the CVs of PtPdNPs decorated RGOs and bare electrode in 0.5 M NaOH solution. Two potential peaks observe during the sweep in the positive direction, which corresponds to dissimilar electrochemical processes that occur on the surface of the PtPdNPs electrode. The peak that lies around -0.65 V is the consequence of the oxidation of the adsorbed hydrogen [32]. Another small peak that appears in the potential range between -0.1 V to 0.15 V may be assigned to the creation of an oxide layer on the surface of the electrode. Still now, the mechanism of the oxidation process is not clear, OH^- has been widely confessed to date to be the first chemisorbed in the primary stage of the oxide production and then changed into higher valence oxides at higher potentials [33]. A wide peak is present in the potential range between 0.0 V to -2.5 V, which contributes to the reduction of metallic oxides during the sweep in the negative direction [24, 34]. Fig. 5B clearly shows that PtPdNPs decorated RGOs-modified electrodes showed a higher catalytic activity than that of PtPdNPs decorated bare plain electrode. The background current of PtPdNPs decorated RGOs-modified electrodes can be seen to be higher than that of PtPdNPs-modified bare plain electrode. These results reveal that when the electrode is modified with RGOs, the effective surface area of the electrode increases [35]. In addition, the electron transfer rate (electron conductivity) also increases when the electrocatalysts are deposited on the RGOs-modified electrode, resulting in an enhancement of the catalytic activity of RGOs/PtPdNPs-modified electrodes. The electroactive surface area (ESA) was observed under the CV in 0.5 M H_2SO_4 solution at a scan rate of 50 mV/s. The entire electric charge of hydrogen adsorption and desorption (Q_H) on the metal nanoparticles, which is obtained by integrating the area under the anodic peaks in the hydrogen region is used to determine ESA [24]. By considering the charge per real active area of the catalyst is 0.210 mC/cm^2. The ESA can be determined by (Q_H/0.210) with multiply particles loading. The ESA and nanoparticles loading of different samples are presented in Table 1. The ESA for the RGOs/PtNPs, RGOs/PdNPs, RGOs/PtPdNPs and Au/PtPdNPs electrodes were estimated to be 78.62 mC/g, 135.72 mC/g, 175.45 mC/g and 163.85 mC/g, respectively. The ESA value of electrocatalyst is similar to the reported in the literature previously [43].

Fig. 6A shows the Chronoamperometry curves of the catalysts in 0.5 M NaOH + 2 M ethanol solution at -0.15 V. The current–time response was monitored for working electrodes with

Au/PtPdNPs, RGOs/PtPdNPs, RGOs/PtNPs, and RGOs/PdNPs for 3000 s at -0.15 V. The polarization currents at PtNPs and PdNPs catalysts consumed quickly during the beginning period.

Table 1. The ESA of different electrocatalysts and nanoparticles loadings.

Catalyst	Nanoparticles loading on electrode (mg/cm^2)	Q_H (mC)	ESA (mC/g)
RGO/PtNPs	0.13	10.22	78.62
RGO/PdNPs	0.22	29.86	135.72
RGO/PtPdNPs	0.31	54.39	175.45
Au/PtPdNPs	0.27	44.24	163.85

However, the current at Au electrode modified with RGOs/PtPdNPs slowly consumed. The rapid reducing current is related to the surface poisoning initiated by the intermediate species, and the lower current consume rate of RGOs/PtPds may be due to the effective removal of the poisons on the electrode surface, which is compatible with the CV curves in Fig. 6A, which is in good agreement with a previous report [36].

The current density for Au/PtPdNPs, RGOs/PtPdNPs, RGOs/PdNPs, and RGOs/PtNPs were also observed to remain at 1.55 mA/cm^2, 2.44 mA/cm^2, 0.62 mA/cm^2, and 0.002 mA/cm^2, respectively, for duration of 3000 s.

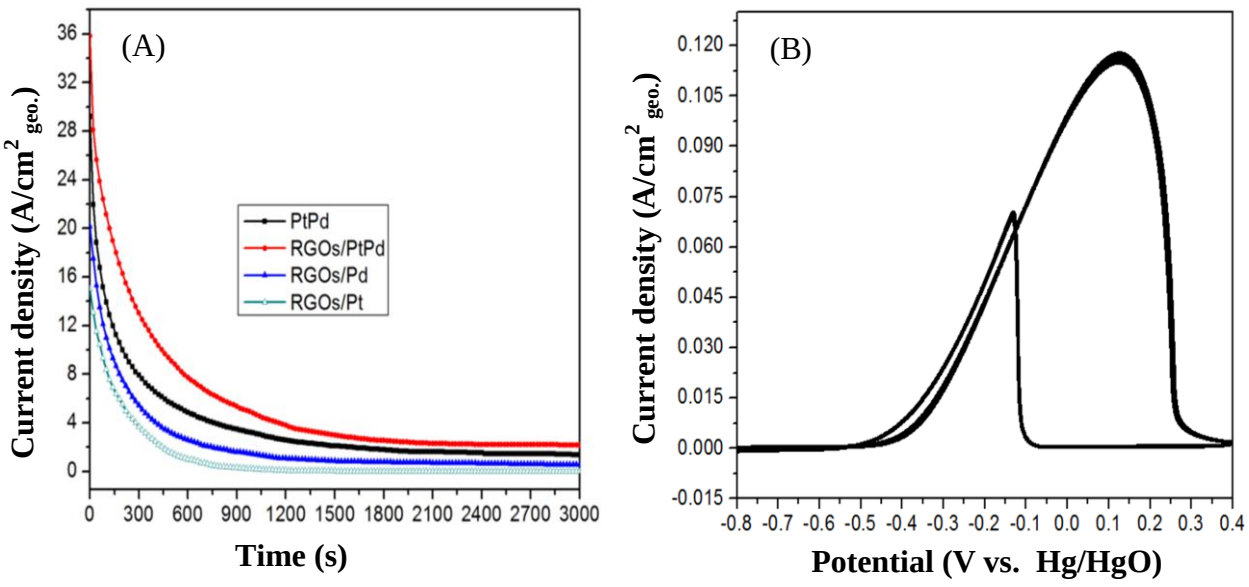

Figure 6. (A) Chronoamperometric curves for ethanol electro-oxidation of various fabricated electrodes in 0.5 M NaOH + 2 M ethanol and (B) catalytic stability of the RGOs/PtPdNPs decorated electrodes for ethanol in 0.5 M NaOH + 2 M ethanol solution at a scan rate of 50 mV/s.

The remaining current density of RGOs/PtPdNPs is higher than that of monometallic nanoparticles catalyst-modified electrodes, suggesting a higher and more stable catalytic activity of the alloy nanoparticles in the given solution. The current density of RGOs/PtPdNPs is also seen to be larger than that of the PtPdNPs decorated bare plain electrode. This consequence reveals that RGOs with PtPd nanoparticles can successfully improve the oxidation of ethanol to CO, and this is assigned to the good charge transfer phenomena of RGOs.

Table 2. Performance of various catalysts for ethanol oxidation.

Electrocatalysts	Onset potential (V)	Current density (mA/cm^2)	Electrolyte	Ref.
Steel/Pd-Ag	-0.80 (SCE)	5.17	Ethanol/NaOH	[4]
GCE/Gr-Nf/PdPt	-0.73 (Ag/AgCl)	7.69	Ethanol/NaOH	[24]
GCE/C/PdNi	-0.80 (MMO)	0.00413	Ethanol/NaOH	[37]
Cu-Ni/PTFE/PtRu	-(MMO)	115	Ethanol/KOH	[38]
$Au/Al_2O_3/Ni$	-(Ag/AgCl)	114	Ethanol/KOH	[39]
GCE/Pd/CNT/Ni	-0.635 (SCE)	-	Ethanol/KOH	[40]
GCE/RGOs/PtAu	-0.786 (SCE)	59	Ethanol/KOH	[41]
GCE/GO-AuPd	-(SCE)	13.16	Ethanol/KOH	[42]
Au/PtPd	-0.63 (MMO)	97.37	Ethanol/NaOH	This work
Au/RGOs/PtPd	-0.671 (MMO)	120.2	Ethanol/NaOH	This work

The stability test of the RGOs/PtPdNPs catalyst toward ethanol electroxidation was conducted through a CV test for 30 cycles in 0.5 M NaOH + 2 M ethanol solution as shown in Fig. 6B. The current density was retained at about 96.75% of the original, indicating that the catalysts exhibit

excellent stability for ethanol electroxidation. It is clear that the alloy catalysts have excellent tolerance against poisoning species when active in the respective solution. In Table 2, the results obtained in this study are compared against those previously reported in the literature. The as-prepared RGOs/PtPdNPs is observed to be a good catalyst for ethanol oxidation.

4. CONCLUSIONS

Reduced graphene oxide sheets (RGOs) were successfully developed by chemical and heat treatment on a gold thin-film electrode. Then PtPdNPs were successfully electrochemically deposited on the RGOs-modified and on bare electrodes. The catalytic performance of the catalyst was evaluated by considering the supporting material. The RGOs-supported PtPd alloy nanoparticles showed a much better catalytic activity for ethanol electroxidation than did bare PtPd or monometallic PtNPs and PdNPs catalysts. In addition, RGOs proved to be a highly effective support for the catalysts due to the promotion of the high electron transfer kinetics. The as-prepared catalyst showed a high current density that can lead to practical applications in anodic catalyst of direct ethanol fuel cells.

ACKNOWLEDGEMENT
This research was partially covered by a research grant from the International Collaborative R&D Program of KIAT/MOTIE, funded by the Ministry of Trade, Industry & Energy (MI, Korea) and the Basic Science Research Program (2010-0024618) through the National Research Foundation of Korea (NRF) funded by the Ministry of Education, Science and Technology.

References

1. L. F. Dong, R. R. S. Gari, Z. Li, M. M. Craig and S. F. Hou, *Carbon*, 48 (2010) 781.
2. Z. Ji, G. Zhu, X. Shen, H. Zhou, C. Wu and M. Wang, *New J. Chem*., 36 (2012) 1774.
3. J. Seweryn and A. Lewera, *J. Power Sources*, 205 (2012) 264.
4. M. C. Oliveira, R. Rego, L. S. Fernandes and P. B. Tavares, *J. Power Sources*, 196 (2011) 6092.
5. F. Kadirgan, S. Beyhan and T. Atilan, *Int. J. Hydrogen Energy*, 34 (2009) 4312.
6. G. Q. Lu, A. Crown and A. Wieckowski, *J. Phys. Chem. B*, 103 (1999) 9700.
7. F. Ksar, L. Ramos, B. Keita, L. Nadjo, P. Beaunier and H. Remita, *Chem. Mat.*, 21 (2009) 3677.
8. G. Eda, G. Fanchini and M. N. Chhowalla, *Nanotech.*, 3 (2008) 270.
9. Y. Hernandez, V. Nicolosi, M. Lotya, F.M. Blighe, Z. Sun, S. De, I. T. Mcgovern, B. Holland, M. Byrne, Y. K. Gun'Ko, J. J. Boland, P. Niraj, G. Duesberg, S. Krishnamurthy, R. Goodhue, J. Hutchison, V. Scardaci, A. C. Ferrari and J. N. Coleman, *Nature Nanotechnology*, 3 (2008) 563.
10. H. Wang, Q. Hao, X. Yang, L. Lu and X. Wang, *Electrochem. Commun*., 11 (2009) 1158.
11. Z. S. Wu, D. W. Wang, W. Ren, J. Zhao, G. Zhou, F. Li and H. M. Cheng, *Adv. Func. Mat*., 20 (2010) 3595.
12. Y. Li, L. Tang and J. Li, *Electrochem. Commun.*, 11 (2009) 846.
13. L. Tang, Y. Wang, Y. Li, H. Feng, J. Lu and J. Li, *Adv. Func. Mat*., 19 (2009) 2782.
14. A. G. Pandolfo and A. F. Hollenkamp, *J. Power Sources*, 157 (2006) 11.
15. E. Y. L. Teo, H. N. Lim, R. Josea and K. F. Chong, *RSC Adv*., 5 (2015) 38111.
16. G. K. Ramesha, S. Sampath, *J Phys. Chem. C*, 113 (2009) 7985.
17. H. K Jeong, Y. P. Lee, M. H. Jin, E. S. Kim, J. J. Bae and Y. H. Lee, *Chem. Phys. Lett*., 470 (2009) 255.
18. W. S. Hummers and R. E. Offeman, *J. Am. Chem. Soc*., 80 (1958) 1339.

19. M. F. Hossain and Jae Y. Park, *RSC Adv*., 3 (2013) 16109.
20. Y. Zhu, M. D. Stoller, W. Cai, A. Velamakanni, R. D. Piner, D. Chen and R. S. Ruoff, ACS Nano, 4 (2010) 1227.
21. Y. Xu, H. Bai, G. Lu, C. Li and G. Shi, *Journal of American Chemical Society*, 130 (2008) 5856.
22. H. Gao, S. Liao, Z. Liang, H. Liang and F. Luo, *J. Power Sources*, 196 (2011) 38.
23. J. Yang, S. Deng, J. Lei, H. Ju and S. Gunasekaran, *Biosens. Bioelectron*., 29 (2011) 159.
24. X. Yang, Q. Yang, J. Xu and C. S. Lee, *J. Mat. Chem*., 22 (2012) 857.
25. S. Hassan, M. Suzuki, A. A. El-Moneim, *Int. J. Electrochem. Sci*., 9 (2014) 8340.
26. J. Shen, M. Shi, N. Li, B. Yan, H. Ma, Y. Hu and M. Ye, *Nano Res. Let.*, 3 (2010) 339.
27. Y. Wang, J. Liu, L. Liu and D. D. Sun, *Nano Res. Let.*, 6 (2011) 1.
28. V. Loryuenyong, K. Totepvimarn, P. Eimburanapravat, W. Boonchompoo and A. Buasri, *Adv. Mat. Sci. Eng*., 2013 (2013) 923403.
29. T. S. Sreeprasad, M. M. Shihabudheen, K. P. Lisha and T. Pradeep, *J. Haz. Mat*., 186 (2011) 921.
30. M. F. Hossain, J. Yin and J. Y. Park, *Japan. J. App. Phys*. 53 (2014) 08NC02.
31. R. N. Singh and A. Singh, Int. *J. Hydrogen Energy*, 34 (2009) 2052.
32. M. Grden, J. Kotowski and A. Czerwinski, *J. Solid State Electrochem*., 7 (2002) 43.
33. Z. X. Liang, T. S. Zhao and J. B. Xu, *Electrochim. Acta*, 54 (2009) 2203.
34. J. B. Xu, T. S. Zhao, Y. S. Li and W. W. Yang, *Int J. Hydrogen Energy*, 35 (2010) 9693.
35. W. Liang and Y. Zhuobin, *Sensors*, 3 (2003) 544.
36. K. Ding, Y. Wang, H. Yang, C. Zheng, Y. Caoa, H. Wei,Y. Wang and Z. Guo, *Electrochim. Acta*, 100 (2013) 147.
37. Z. Zhang, L. Xin, K. Sun and W. Li, *Int. J. hydrogen energy*, 36 (2011) 12686.
38. S. S. Gupta and J. Datta, *J. Power Sources*, 145 (2005) 124.
39. J. J. Huang, W. S. Hwang, Y. C. Weng and T. C. Chou, *Materials Transactions*, 50 (2009) 1139.
40. R. N. Singh and A. S. Anindita, *Carbon*, 47 (2009) 271.
41. Z. Huang, H. Zhou, C. Li, F. Zeng, C. Fua and Y. Kuang, *J. Mater. Chem.*, 22 (2012) 1781.
42. Q. Wang, X. Cui, W. Guan, X. Zhang, C. Liu, T. Xue, H. Wang and W. Zheng, *Microchim Acta*, 181 (2014) 373.
43. A. Pozio, M. D. Francesco, A. Cemmi, F. Cardellini and L. Giorgi, *J. Power Sources*, 105 (2002) 13.